Supporting Information

Mobile Media Promotes Orientation of 2D/3D Hybrid Lead Halide Perovskite for Efficient Solar Cells

Ning Zhou[a], *Yu Zhang*[a], *Zijian Huang*[a], *Zhenyu Guo*[a], *Cheng Zhu*[b], *Jingying He*[c], *Qi Chen*[b], *Wentao Sun*[c], *Huanping Zhou**[a]

a. Beijing Key Laboratory for Theory and Technology of Advanced Battery Materials, Key Laboratory of Polymer Chemistry and Physics of Ministry of Education, BIC-ESAT, School of Materials Science and Engineering, Peking University, Beijing 100871, P. R. China
b. School of Materials Science and Engineering, Beijing Institute of Technology, Beijing 100081, P. R. China
c. Key Laboratory for the Physics and Chemistry of Nano devices, Department of Electronics, Peking University, Beijing 100871, P. R. China

E-mail: happy_zhou@pku.edu.cn

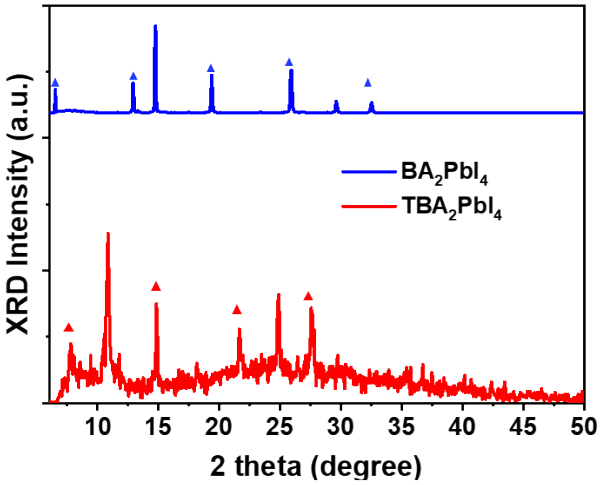

Figure S1. The XRD spectra of BA_2PbI_4 and TBA_2PbI_4.

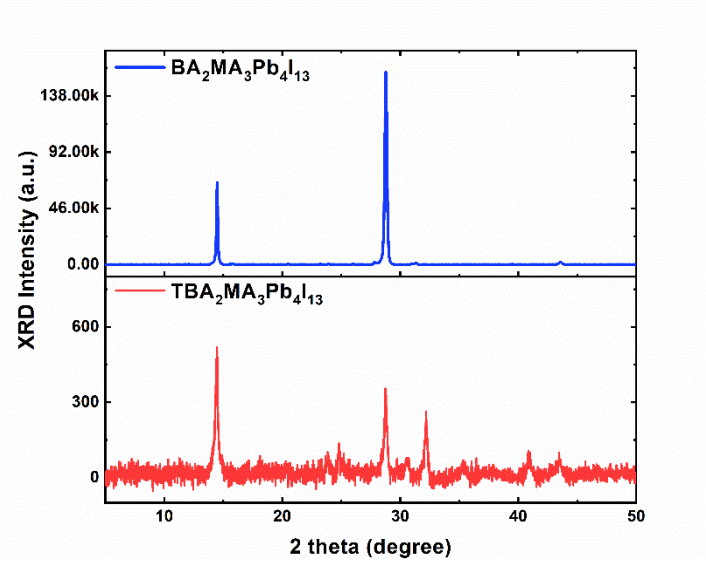

Figure S2. XRD patterns of $BA_2MA_3Pb_4I_{13}$ and $TBA_2MA_3Pb_4I_{13}$ films based on hot-casting method.

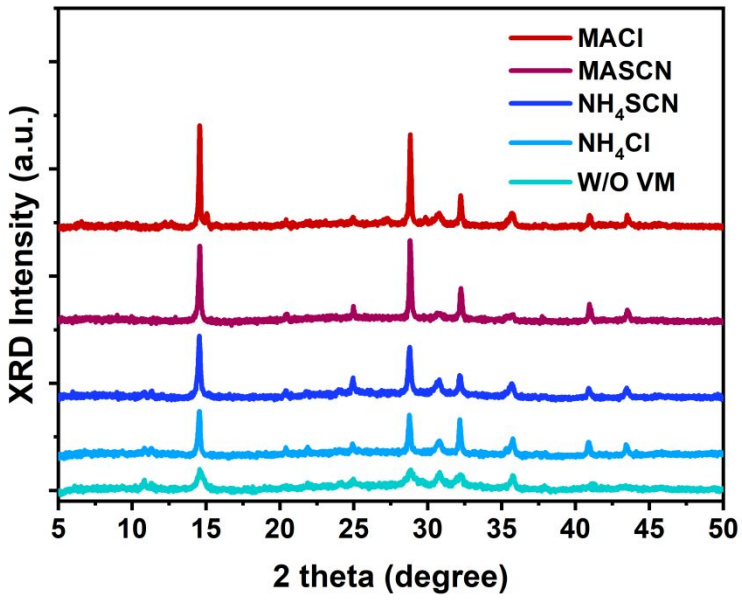

Figure S3. XRD patterns of the films without or with different volatile salts based on $(TBA)_2(MA)_3Pb_4I_{13}$ perovskite films.

Table S1. The FWHM and integral peak area derived from the XRD results.

	W/O VM	NH_4Cl	NH_4SCN	MASCN	MACl
FWHM of （111）/°	0.299	0.104	0.091	0.088	0.078
Peak area of (111)	725	2108	2552	6822	18234

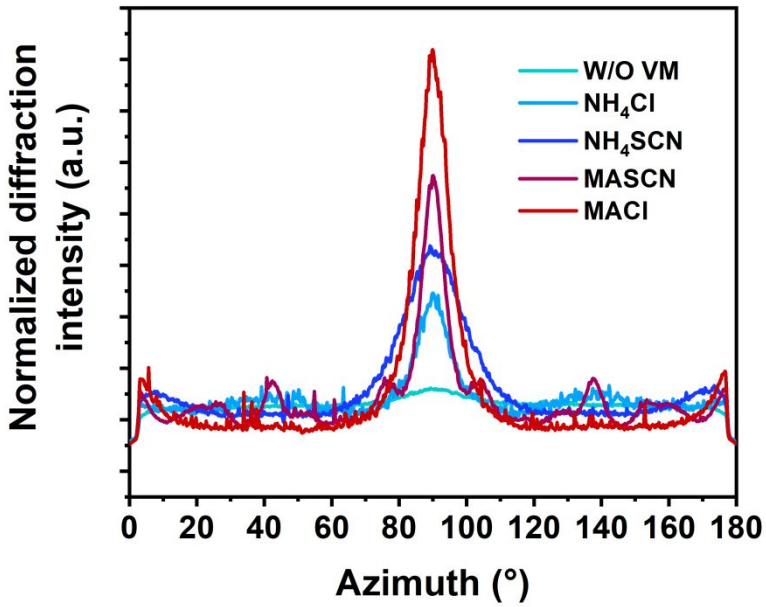

Figure S4. Integrated intensity plots azimuthally along the ring at $q_{xy} \approx -1$ to 1 $Å^{-1}$.

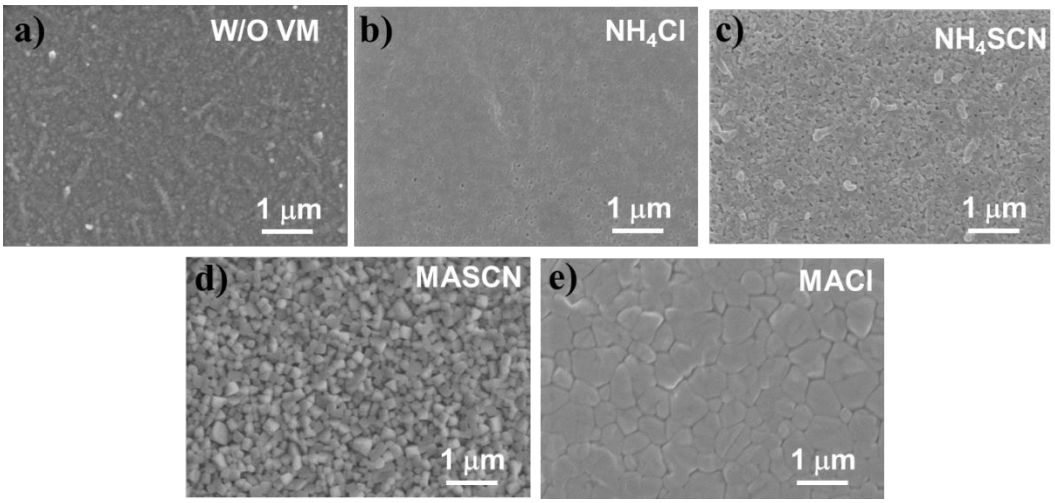

Figure S5. (a) SEM images of the 2D/3D hybrid perovskite films without volatile salts; (b)-(e) SEM images of the 2D/3D hybrid perovskite films with the assistance of NH_4Cl, NH_4SCN, MASCN, MACl, respectively.

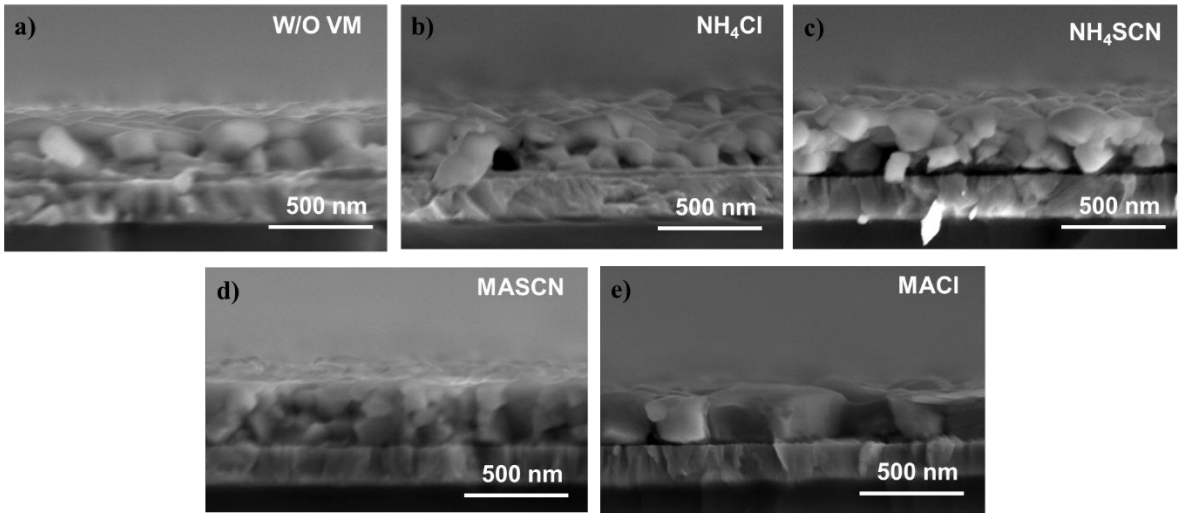

Figure S6. (a)The cross-sectional SEM images of the 2D/3D hybrid perovskite films without volatile salts; (b)-(e) SEM images of the 2D/3D hybrid perovskite films with the assistance of NH_4Cl, NH_4SCN, MASCN, MACl, respectively.

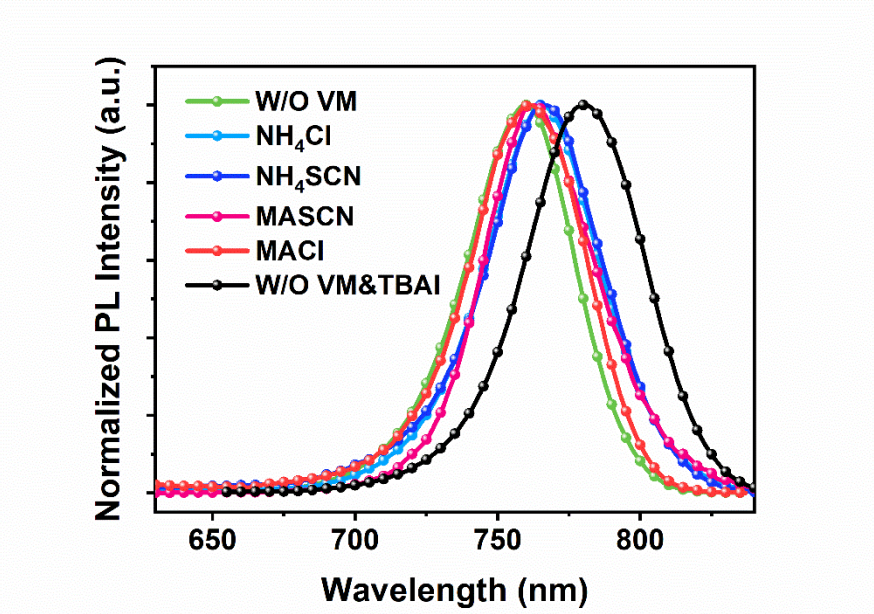

Figure S7. The steady-state PL spectra of the $TBA_2MA_9Pb_{10}I_{31}$ perovskite films with different volatile salts.

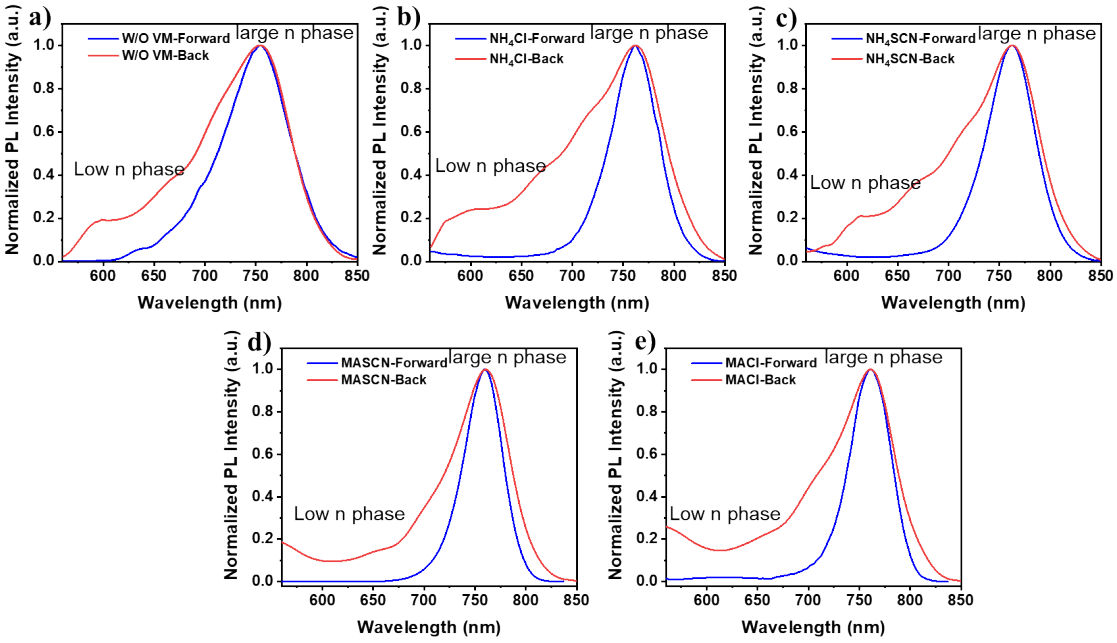

Figure S8. (a) The front and back PL of the 2D/3D hybrid perovskite films (ITO/perovskite) without volatile salts; (b)-(e) The front and back PL of the 2D/3D hybrid perovskite films with the assistance of NH_4Cl, NH_4SCN, MASCN, MACl, respectively.

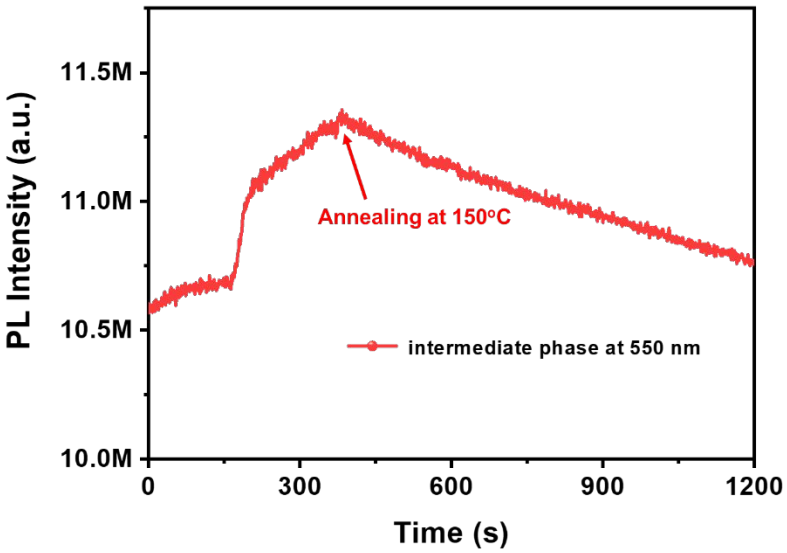

Figure S9. *In situ* PL measurement for $TBA_2MA_9Pb_{10}I_{31}$ film formation process with MACl by detecting the emission peak at 550 nm.

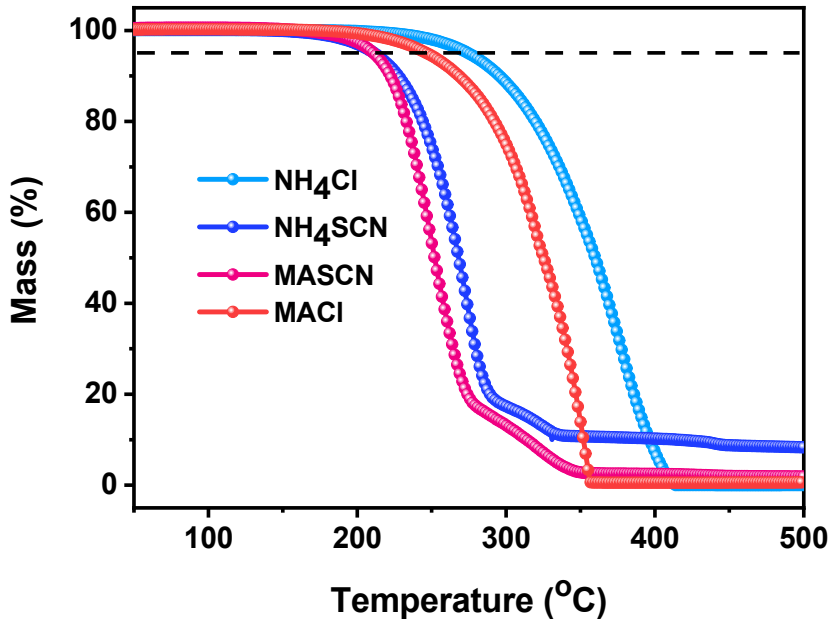

Figure S10. TGA curves for NH_4Cl, NH_4SCN, MASCN, MACl, respectively in nitrogen atmosphere.

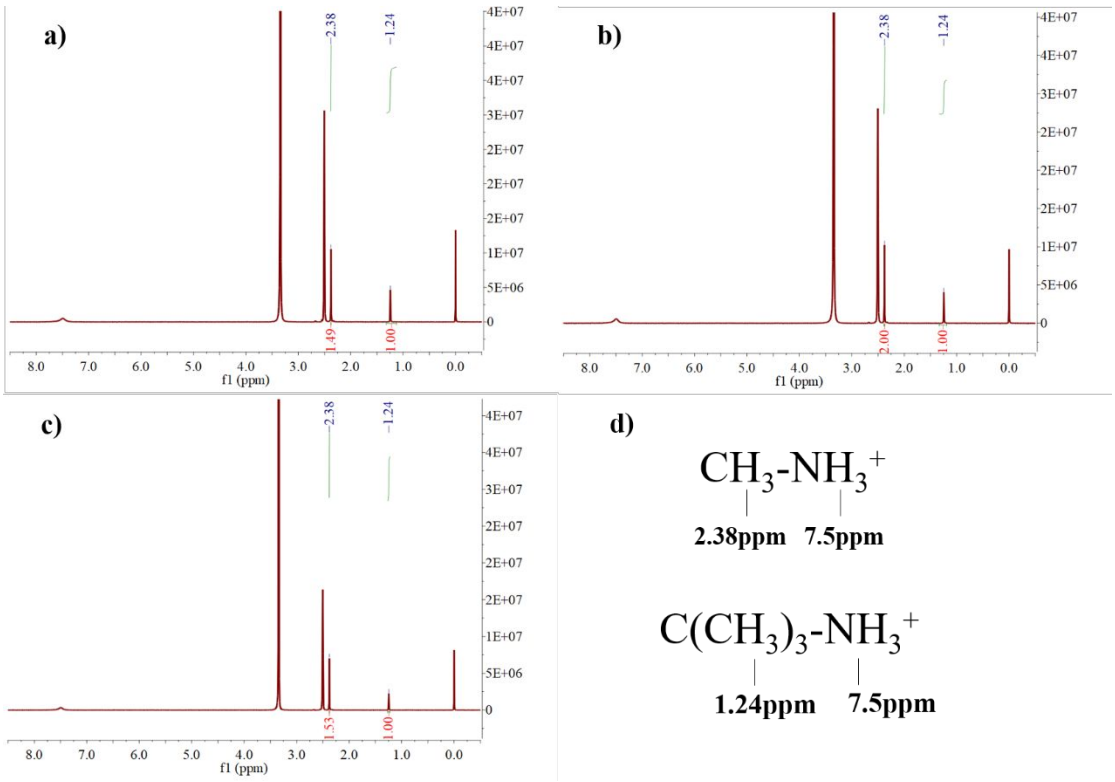

Figure S11. The NMR spectra of (a) $TBA_2MA_9Pb_{10}I_{31}$ without volatile salte; (b) $TBA_2MA_9Pb_{10}I_{31}$ with MASCN; (c) $TBA_2MA_9Pb_{10}I_{31}$ with MACl; (d) The chemical shift of the H from the different organic cations. The samples were scraped from the formed films.

The chemical shift located at 0 ppm、~2.51 ppm、~3.32 ppm represented $Si(CH_3)_4$, dimethyl sulfoxide-d6, H_2O, respectively. The chemical shift of H bonding with C in $CH_3NH_3^+$ located at 2.38 ppm, and the chemical shift of H bonding with C in $C(CH_3)_3NH_3^+$ located at 1.24 ppm, where the chemical shift of H bonding with N in both $CH_3NH_3^+$ and $C(CH_3)_3NH_3^+$ located at 7.5 ppm.

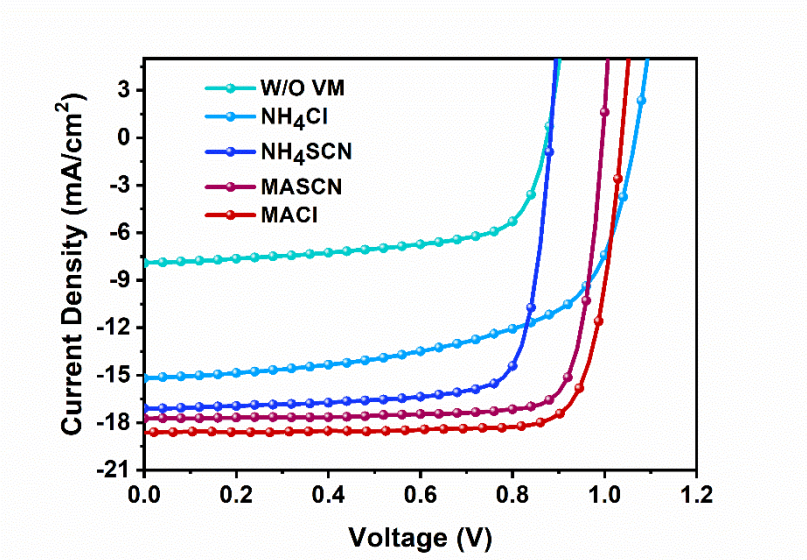

Figure S12. The J-V curves of $TBA_2MA_9Pb_{10}I_{31}$ with or without volatile salts based perovskite solar cells by adopting invert device structure.

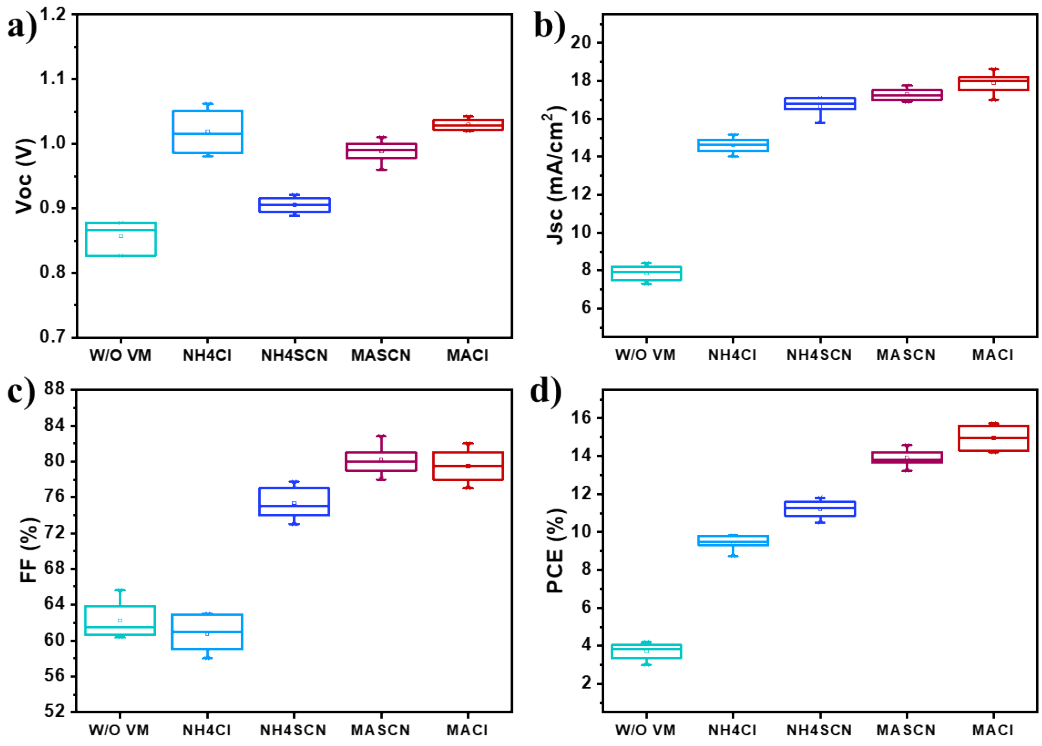

Figure S13. (a) Voc; (b) Jsc; (c) FF; (d) PCE statistic distribution of 2D/3D hybrid perovskite based solar cells without volatile salts and with the assistance of NH_4Cl, NH_4SCN, MASCN, MACl, respectively.

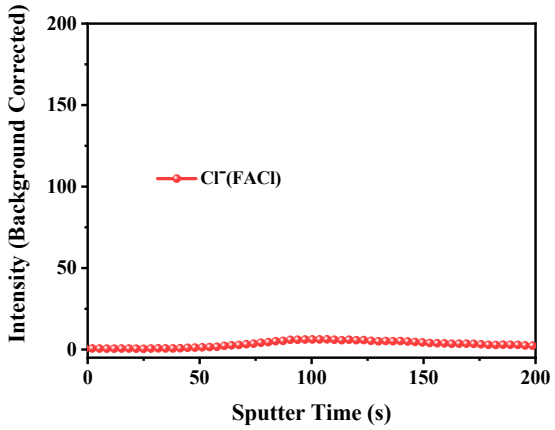

Figure S14. TOF-SIMS depth-profiles of film with FACl.

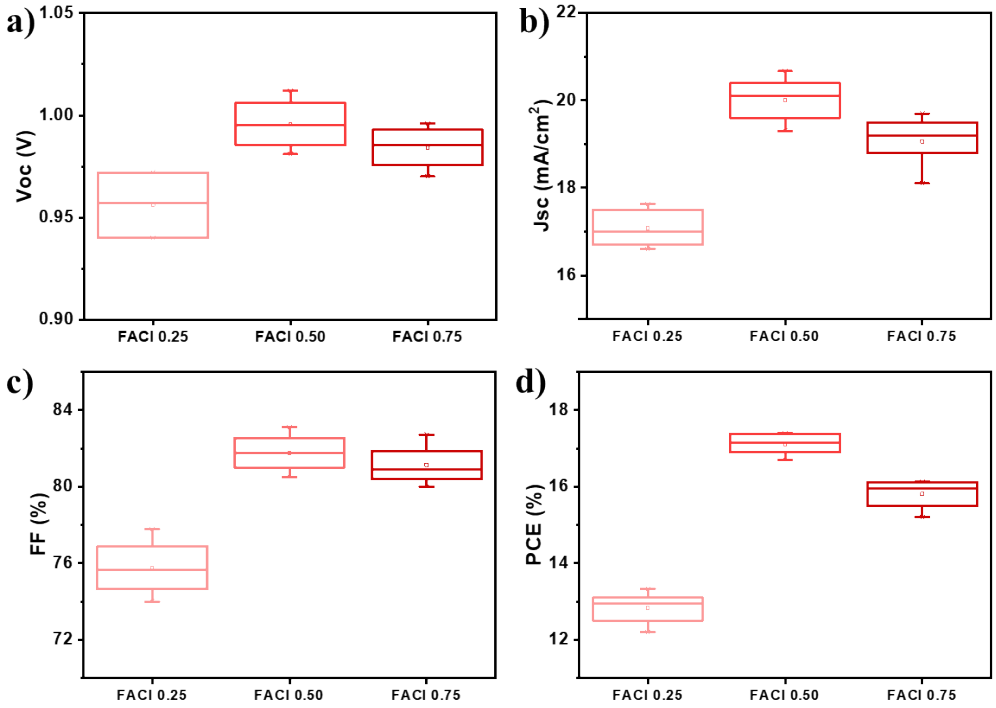

Figure S15. (a) Voc; (b) Jsc; (c) FF; (d) PCE statistic distribution of 2D/3D hybrid perovskite based solar cells with the assistance of FACl 0.25, FACl0.50, FACl 0.75, respectively.

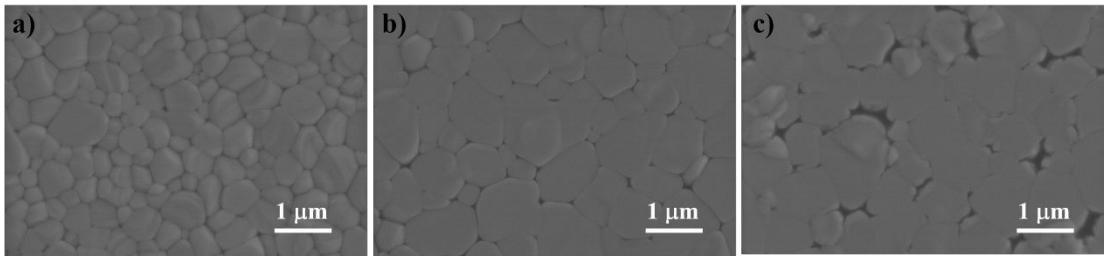

Figure S16. (a)-(c) SEM images of the 2D/3D hybrid perovskite films with the assistance of FACl0.25, FACl50, FACl0.75, respectively.

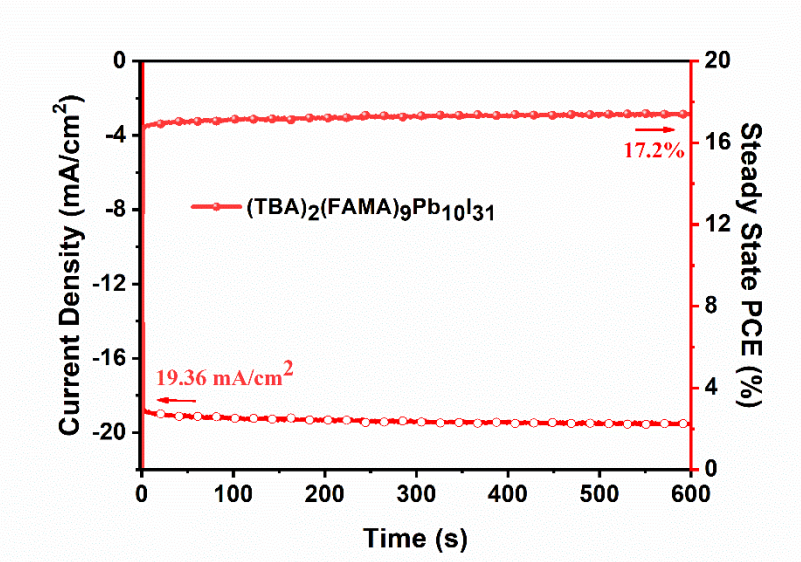

Figure S17. The steady-state PCE of the $TBA_2MA_9Pb_{10}I_{31}$ (17.2% at a voltage of 0.89V) based perovskite solar cells.

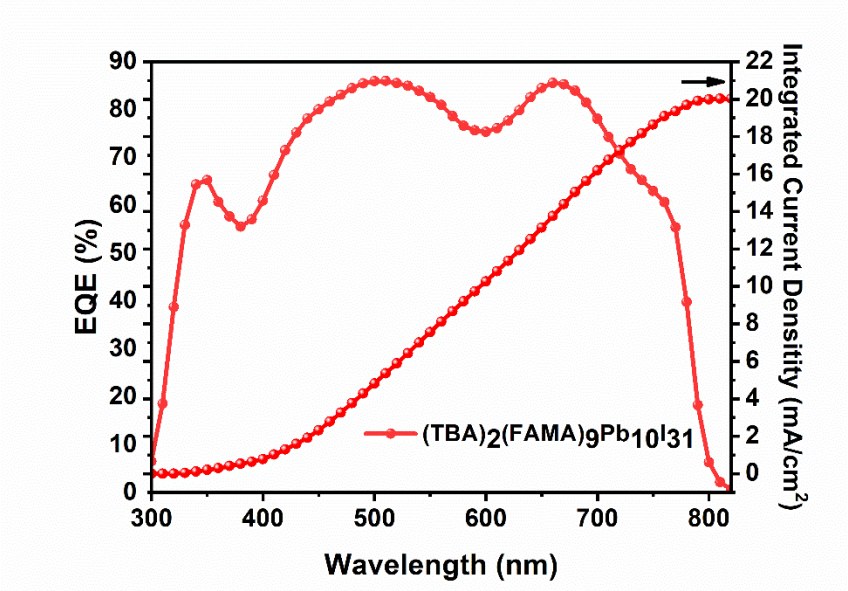

Figure S18. The EQE spectra of $TBA_2(FAMA)_9Pb_{10}I_{31}$ based perovskite solar cells.

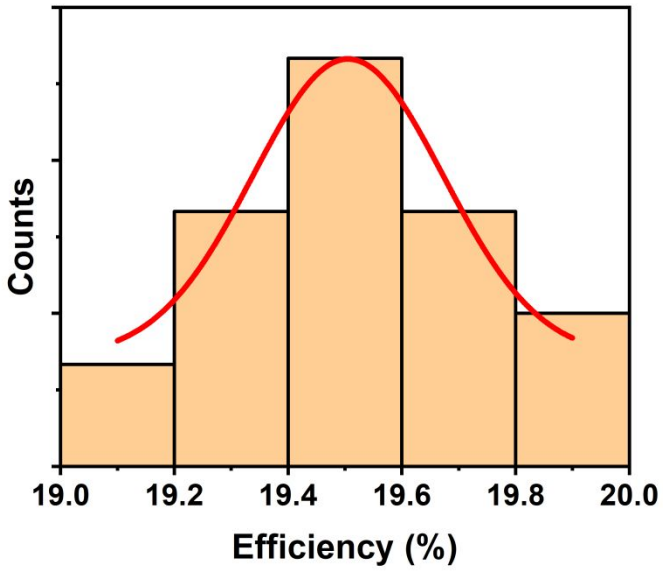

Figure S19. Histograms of PCE for $TBA_2MA_{19}Pb_{20}I_{61}$ based solar cells, composed of 23 separate devices.

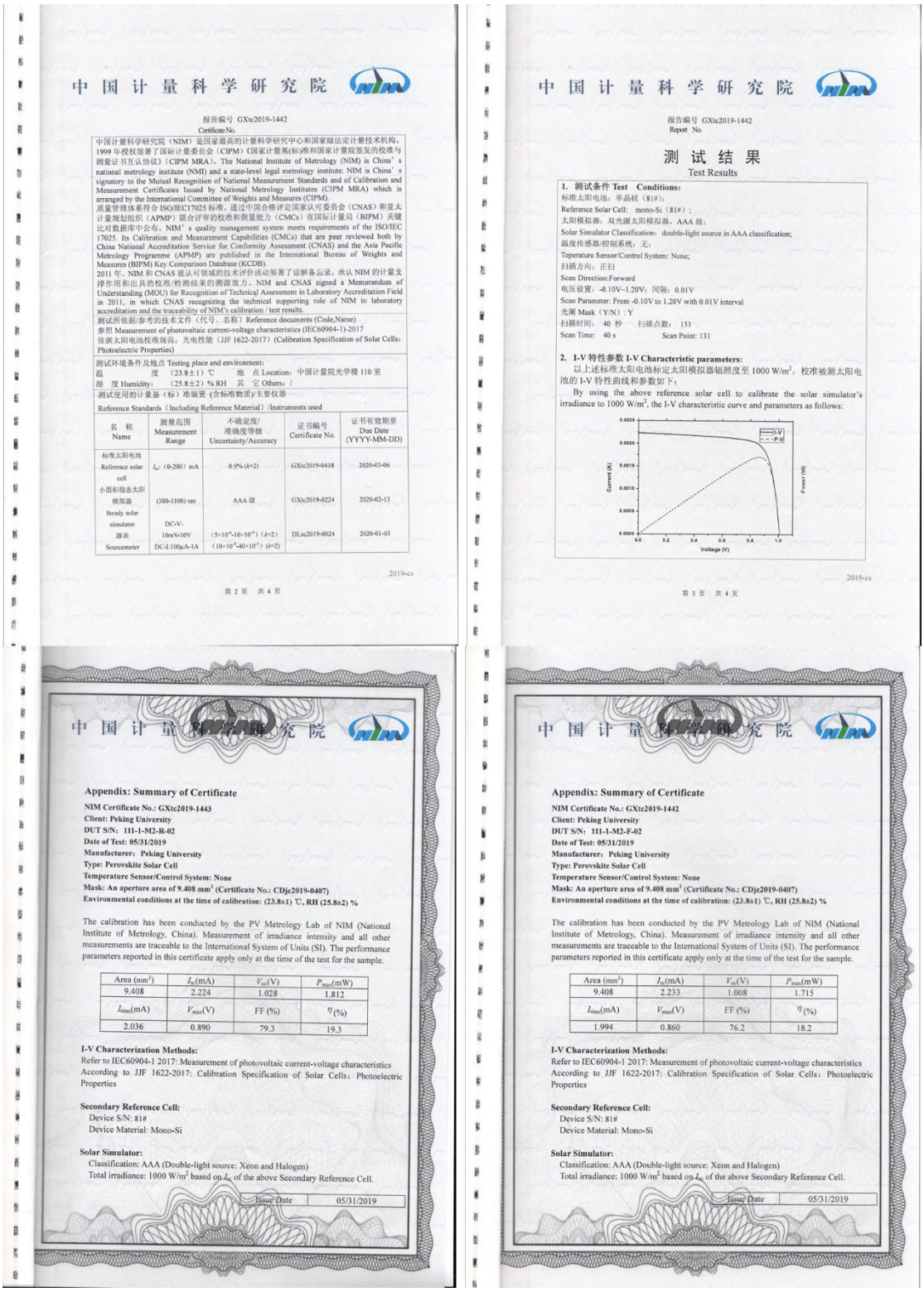

Figure S20. Certificated results by the National Institute of Metrology, China (NIM, China). The forward scan is performed from –0.1 V to 1.2 V at 33 mV/s, with a PCE of 18.2% (Voc =1.008 V, Isc=2.233 mA, FF=76.2%). The reverse scan is performed from 1.2 V to –0.1 V at 33 mV/s, with a PCE of 19.3% (Voc=1.028 V, Jsc=2.224 mA, FF=79.3%). The device has an active area of 0.09408 cm^2.

.

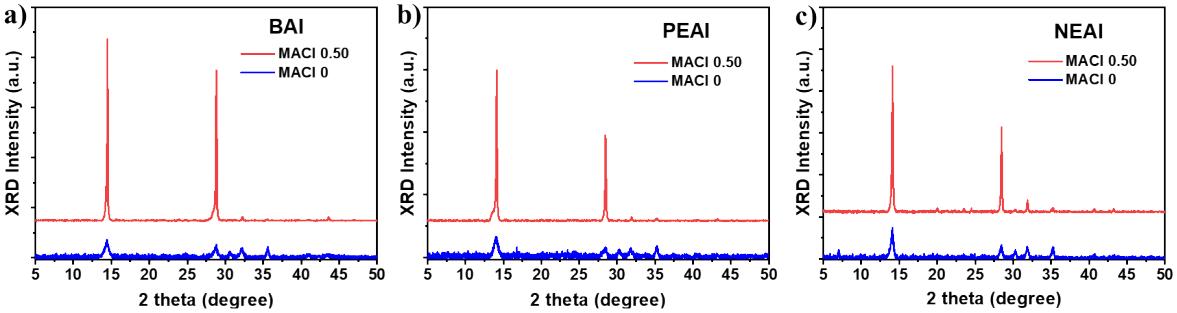

Figure S21. (a) XRD patterns of the $(BA)_2(MA)_9Pb_{10}I_{31}$ perovskite films without and with MACl. (b) $(PEA)_2(MA)_9Pb_{10}I_{31}$ without and with MACl. (c) $(NEA)_2(MA)_9Pb_{10}I_{31}$ without and with MACl.